# WEB LENGTH CREEP IN WOUND ROLLS

**By**

**C. Mollamahmutoglu[1], A. Gajjalla[2], R. Markum[2], A. Azoug[2] and J. K. Good[2]**
**[1]Yildiz Technical University, TURKEY**
**[2]Oklahoma State University, USA**

## ABSTRACT

For convenience, webs are stored in wound rolls. The available web length in a wound roll is one mark of roll quality and a concern for many who process and convert webs. Elastic winding models have proven very precise at estimating the number of layers, the web length wound into a roll, and the residual stresses in the roll at the time of winding. Wound rolls can spend long periods of time in storage, where controlling the environment is cost-prohibitive. As many webs are viscoelastic on some time scale, the residual stresses due to winding will result in creep during storage. The changes in web length due to creep result in web process errors and quality loss, including registration errors and camber webs for example. This publication will focus on the development of a viscoelastic winding model to predict these changes in web length due to creep in a wound roll. The viscoelastic model predicts the tangential stress relaxation and radial creep due to winding residual stresses from a fully viscoelastic orthotropic material behavior. A spunned-meltblown-spunned (SMS) web and a low-density polyethylene (LDPE) web are taken as examples of viscoelastic webs. Their viscoelastic properties are systematically characterized using creep experiments. The results of the model show good agreement with winding and storage experiments for both webs. Finally, webs often do not creep uniformly across their width. An example of this non-uniform creep will be explored.

## INTRODUCTION

The precise diagnosis of defects in webs helps mitigate product and economic loss. Common sources of economic or quality loss in web processes are registration errors and length defects. Registration errors are the misalignment of discrete coatings on a web. They can occur when discrete coatings must be positioned accurately with respect to previous coatings. This is readily apparent when graphics or electronics are deposited at precise intervals prior to winding and roll storage. In a subsequent web process, the web is unwound and the total web length has changed nonuniformly down the web length.

Thus, the interval between graphics or electronics is no longer constant and results in registration conversion error.

Length defects are characterized as varied forms of web length variation across the width. A web can have a *baggy center* as a result of having longer web length at the widthwise center [1]. Likewise, a web can have *baggy edges* due to the edges being longer than the center. *Web camber* results from a linear variation in length over the web width. These length defects cause process defects. A web that is not planar is difficult to coat uniformly. If the web tension is increased to achieve planarity, then the tension is not constant across the web width, which will result in a nonuniform coating thickness. Webs are formed in roll-to-roll machines that should be able to achieve very good length uniformity over the web width. The leading cause of length nonuniformity of webs is the nonuniformity of web thickness that is much more difficult to control in the formation process. The thickness nonuniformity combined with viscoelastic behavior and requirements that webs be wound and stored produces *baggy center*, *baggy edge*, *baggy lane* and *web camber* length defects [1].

The origin of both registration errors and length defects is a change in length in the web, most often due to viscoelastic phenomena in wound rolls (Figure 1). All webs are viscoelastic on some time scale and creep can be expected during the roll-to-roll process or while the wound roll is in storage. The creep phenomenon is the increase in strain resulting from a constant applied loading. In the case of webs, web tension and residual stresses in the wound roll subject the web to a significant load over long times, which leads to an increase in length in the direction of the loading. The phenomenon of stress relaxation is the decrease of the stress at constant strain. Although tangential and radial creep and stress relaxation phenomena are coupled, stress relaxation happens mainly in the tangential direction in a roll wound under tension (Figure 1).

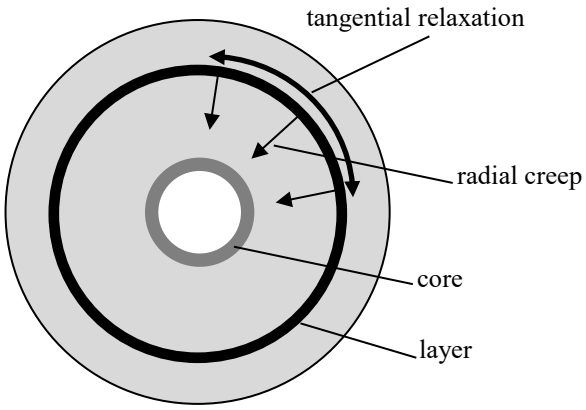


Figure 1 – Interaction of Radial Creep and Tangential Relaxation in a Roll

Roll-to-roll manufacturing processes are time-dependent, although the process time is generally much shorter than the storage time. Web processes are often speed-limited, examples include discrete printings and coatings which require time to dry before contact with rollers. Coatings are formulated with solvents that can range from water to hydrocarbons, whose drying times vary widely. In addition, products made in roll-to-roll manufacturing processes often require the web to be unwound and rewound several times before the web is converted to a deliverable product. The web is stored in wound rolls

between steps of the process. For example, a product can require the deposition of one or more coatings involving solvents with various drying times, dictating a unique web velocity. This requires the web to be unwound and rewound multiple times while the web awaits unwinding in the next process. Creep in webs mainly occur over storage periods, which are significantly longer than the process periods. In addition, the storage temperature and humidity are not controlled because of the cost of controlling the environment in large warehouses. Both temperature and humidity may contribute to accelerate or decelerate the creep phenomenon.

Finally, in narrow webs with little thickness variation, this deformation occurs uniformly across the web width. However, heterogeneities in the web and in applied load will lead to heterogeneous inelastic deformations. An efficient model needs to consider this heterogeneity and cannot be limited to a simple 1D representation of the problem.

These deformation-related defects provide the stimulus for the development of deformation-based winding models that allow exploration of uniform and nonuniform creep resulting in web defects. Elastic winding models are now at a mature stage of development [2]. The one-dimensional (1D) winding models originally developed allowed the exploration of radial pressure and tangential stresses as functions of wound roll radius. As these models evolved, they became more accurate and useful for predicting stress-related defects [3,4]. Deformations within wound rolls were first approached with the objective of discerning how they affected the stresses [5-7]. Interest then developed with regard to how viscoelastic web material behavior affected the residual stresses due to winding [8-11]. Eventually, researchers addressed manufacturing imperfections in the webs. The non-uniformity of the web in thickness and length when entering a winding roll caused spatial variation in the winding residual stresses. This spawned the development of a series of two dimensional (2D) models that allowed radial pressure, as well as tangential, axial, and shear stresses to be explored as a function of radius and widthwise location in the wound roll [12-17].

The model developed here will be a 2D axisymmetric winding model which allocates winding tension as a function of the variation of the wound roll radius across the roll width combined with viscoelastic material behavior during storage.

## MODEL DEVELOPMENT

The analysis is divided into two phases: the winding phase (elastic) and the storage phase (viscoelastic). Experience has shown elastic winding models that account for the state-dependency of the radial modulus provide accurate results just after winding for a range of materials (newsprint, LDPE, polyester, tissue, nonwovens) [2,9,10]. Although all webs exhibit viscoelastic behavior on some time scale, this time scale is larger than the winding time scale. Thus, in the first phase of analysis, the time of winding is considered insignificant compared to the storage time and winding is reasonably modeled as elastic. The output of the first phase is the elastic residual stress due to winding. This elastic residual stress becomes the initial stress in the second phase. The second phase analyzes the viscoelastic creep that occurs during storage.

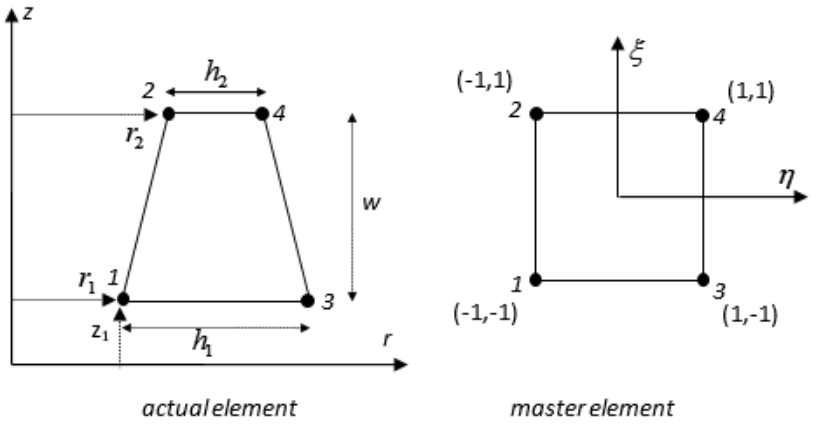


Figure 2 – Four node quadrilateral element

**Phase One: Elastic Winding Mechanics**

A 2D axisymmetric finite element elastic winding model is posed. 2D formulations are superior to previous 1D formulations as problems involving web thickness and length variation can be attacked. Even when web thickness or length does not vary appreciably, 2D formulations allow the web material properties and winding conditions to dictate whether plane stress, plane strain or intermediate conditions exist without requiring further assumption. A four-node axisymmetric quadrilateral element is considered as shown in Figure 2. An incoming layer to the winder is modeled with these axisymmetric quadrilaterals in Cross Machine Direction (CMD) as shown in Figure 3.

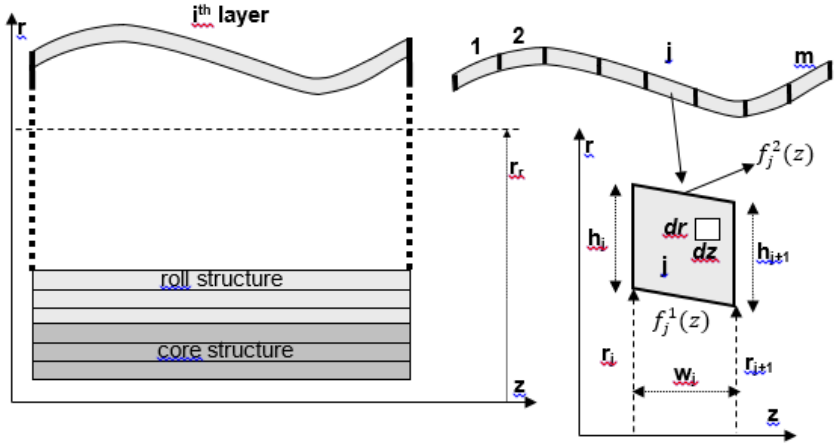


Figure 3– Web layer modelling with Quad elements in CMD

The general stiffness and force elemental matrices for axisymmetric winding models have been developed in previous publications [14,15]. The element stiffness matrix and force vector are written as:

$$K_e u_e = F_e \qquad \{1\}$$

$$K_e = \int_{-1}^{1}\int_{-1}^{1} B^T M_e B \det[J] r d\eta d\xi \qquad \{2\}$$

$$F_e = \int_{-1}^{1}\int_{-1}^{1} B^T (\sigma_o)_e \det[J] r d\eta d\xi \qquad \{3\}$$

The displacement vector $u_e$ is an 8 x 1 matrix with 2 degrees of freedom for each of the four nodes of the quadrilateral element. The strain-displacement matrix $B$ relates the four axisymmetric strains $\{\varepsilon_r \quad \varepsilon_z \quad \gamma_{rz} \quad \varepsilon_\theta\}^T$ to the nodal deformations $u_e$. (We point out to the reader that the notation employed is equivalent but not identical to the Voigt notation.) The Jacobian $J$ is used to transform derivatives from the Cartesian coordinates $\{r, z\}$ to the natural coordinates $\{\xi, \eta\}$. The stiffness tensor $M_e$ is the inverse of the compliance tensor $C_e$, which relates the elemental strains $\varepsilon_e$ to stresses $\sigma_e$. For an orthotropic material,

$$C_e = \begin{bmatrix} 1/E_r & -\upsilon_{rz}/E_z & 0 & -\upsilon_{r\theta}/E_\theta \\ -\upsilon_{rz}/E_z & 1/E_z & 0 & -\upsilon_{z\theta}/E_\theta \\ 0 & 0 & 1/G_{rz} & 0 \\ -\upsilon_{r\theta}/E_\theta & -\upsilon_{z\theta}/E_\theta & 0 & 1/E_\theta \end{bmatrix} = M_e^{-1} \text{ and } \begin{Bmatrix} \sigma_r \\ \sigma_z \\ \tau_{rz} \\ \sigma_\theta \end{Bmatrix} = [M]_e \begin{Bmatrix} \varepsilon_r \\ \varepsilon_z \\ \gamma_{rz} \\ \varepsilon_\theta \end{Bmatrix} \qquad \{4\}$$

where $E_i$ is the Young modulus, $G_i$ the shear modulus, and $\upsilon_i$ the Poisson's ratio in the direction $i$. Importantly, the radial Young modulus $E_r$ has been found to be state-dependent on the radial stress, *i.e.* $E_r = E_r(\sigma_r)$. A common form for $E_r$, provided by Pfeiffer [18], was adopted here:

$$E_r = K_2(-\sigma_r + K_1) \text{ and } -\sigma_r = P = K_1\left(e^{K_2\varepsilon_r} - 1\right) \qquad \{5\}$$

*where* $K_1$ and $K_2$ are constants that are obtained by curve fitting pressure versus strain data acquired during web stack compression tests. In a wound roll the radial modulus $E_r$ of each element/layer is unique and will increase as layers are added to the roll during winding. Winding is inherently an accretive layer-wise process which made the employment of stepwise linearization natural. The addition of each layer is a solution step. During each solution of a step, the unique radial moduli of the elements are kept constant.

The force vector development is based on a pre-stress concept presented in equation {3}. In {3}, $(\sigma_0)_e$ is the initial stress for an element $e$ in the MD or $\theta$ direction due to web tensile stress which results from tension in the web incoming to the winder. Selecting an appropriate $(\sigma_0)_e$ vector for an element in order to simulate the effect of thickness variation is discussed in [15,16] in detail. Expression {6} is a statement of the mechanical equilibrium of the outer lap. The left-hand side is the total web line force written in terms of the average web line stress $T_w$ due to tension multiplied by the total cross-sectional area of the web. Here $A_j$ is the area of the sector $j$ (Figure 3). The right-hand side is the total web line force written in terms of the tangential strains due to the roll outer lap radius profile in the CMD or z direction. Here $E_{\theta j}$ is the tangential modulus for sector $j$ and the functions $f_j$ are defined in Figure 2. The strain (integrand) produces a corresponding stress for sector $j$. A key point was expressing the tangential strain

utilizing the relaxation radius $r_r$ concept introduced by Cole and Hakiel [11], that denotes the radius the layer of web would have if it were completely relaxed, meaning tension free. This approach allows the incorporation of the effect of roll outer lap radius variation in the z direction on the pre-stress for each sector.

$$T_w \sum_{j=1}^{m} A_j = \sum_{j=1}^{m} E_{\theta j} \int_0^{w_j} \int_{f_j^1(z)}^{f_j^2(z)} \frac{r - r_r}{r_r} dr dz \qquad \{6\}$$

The relaxation radius is determined by optimization from expression {6}. Inserting the relaxation radius $r_r$ into equation {7}, the appropriate pre-stress vector $(\sigma_0)_e=(\sigma_0)^j$ for each finite element in a new outer layer can be developed which accounts for the effect of CMD thickness non-uniformity.

$$(\sigma_0)^j = \begin{bmatrix} 0 & 0 & 0 & -E_{\theta j} \dfrac{r_j - r_r}{r_r} \end{bmatrix}^t \qquad \{7\}$$

The superscript 'j' in the above equation refers to the $j^{th}$ sector along the CMD direction noted in Figure 3. The obtained pre-stress from expression {7} is inserted into equation {3} to determine the elemental force vectors. The elemental force vectors $F_e$ is assembled into a system force vector $F$ and the current element stiffness matrices $K_e$ is assembled into the system stiffness matrix $K$.

The system stiffness matrix is first defined with the element stiffness terms representing the core and the first layer of web wound onto the core. The set of equations $K\delta u=F$ is then solved for the increment in radial deformation $\delta u$ that resulted from the addition of the first layer.

Subsequently, for each layer $i$ added to the outer surface, the system of equations $K\delta u=F$ is solved for the increments in deformation for all layers in the wound roll. The incremental strains and stresses are then computed for each layer and summed with previous increments to determine the total residual strains and stresses in a wound roll containing $i$ web layers. Finally, the material properties are updated as a function of the total stress. And the process continues to add the layer $i+1$ to the outside of the wound roll until a user designated final wound roll radius is achieved. At that point, the total elastic stress and strain due to the winding process are known and will be used as initial conditions for the viscoelastic analysis in the second phase.

## Phase Two: Viscoelastic Creep in the Wound Roll

**Linear viscoelastic constitutive law.** The web material will be modeled with a linear viscoelastic constitutive law. Linear viscoelastic materials obey the Boltzmann superposition principle, which states that the response of a material to a given load is independent of the response of the material to any load already applied [19]. For linear viscoelastic webs, it is assumed that the Boltzmann superposition principle holds in a modified manner per the pressure-dependence of the radial modulus. This assumption is supported by the fact that the radial strains remain small compared to the tangential strains. In case of an initial stress or strain field due to winding (Phase One), this leads to:

$$\sigma(t) = M(t, P(t))\varepsilon(0) + \int_0^t M(t-\tau, P(\tau)) \frac{\partial \varepsilon}{\partial \tau} d\tau \qquad \{8\}$$

or equivalently:

$$\varepsilon(t) = C(t,P(t))\sigma(0) + \int_0^t C(t-\tau,P(\tau))\frac{\partial \sigma}{\partial \tau} d\tau \quad \{9\}$$

where $\sigma(t)$ and $\varepsilon(t)$ are the time-dependent Cauchy stress and small displacement strain tensors, respectively, $P(t)$ is the radial pressure at time $t$ (i.e. $P(t) = -\sigma_r(t)$), $M(t,P(t))$ is the fourth-order stiffness tensor and $C(t,P(t))$ is the fourth-order compliance tensor of the orthotropic viscoelastic material. Following the notation convention introduced in Phase One, the second-order stress $\sigma(t)$ and strain $\varepsilon(t)$ tensors can be expressed as:

$$(\sigma) = \{\sigma_r \quad \sigma_z \quad \tau_{rz} \quad \sigma_\theta\}^T \quad \{10\}$$

$$(\varepsilon) = \{\varepsilon_r \quad \varepsilon_z \quad \gamma_{rz} \quad \varepsilon_\theta\}^T \quad \{11\}$$

$\sigma(0)$ and $\varepsilon(0)$ are the initial stress and strain tensors, respectively, which exist prior to any viscous event taking place. The viscoelastic compliance tensor $C(t,P(t))$ and the viscoelastic stiffness tensor $M(t,P(t))$ can then be expressed as

$$C(t,P) = \begin{bmatrix} J_r(t,P) & J_{zr}(t,P) & 0 & J_{\theta r}(t,P) \\ J_{rz}(t,P) & J_z(t) & 0 & J_{\theta z}(t) \\ 0 & 0 & J_{rz}(t) & 0 \\ J_{r\theta}(t,P) & J_{z\theta}(t) & 0 & J_\theta(t) \end{bmatrix} \quad \{12\}$$

$$M(t,P) = \begin{bmatrix} E_r(t,P) & E_{zr}(t,P) & 0 & E_{\theta r}(t,P) \\ E_{rz}(t,P) & E_z(t) & 0 & E_{\theta z}(t) \\ 0 & 0 & E_{rz}(t) & 0 \\ E_{r\theta}(t,P) & E_{z\theta}(t) & 0 & E_\theta(t) \end{bmatrix} \quad \{13\}$$

where the functions $J$ are the compliances in the different directions, often called creep functions, and the functions $E$ are the moduli in the different directions, often called relaxation functions.

As observed, the tensors $C$ and $M$ are also a function of the current pressure $P$ at time $t$ due to state-dependency. Consequently, the components of $C$ and $M$ in the radial direction are functions of $P$ in the most general case (equations {12} and {13}). The nature of the components of the compliance tensor and their approximations will be discussed later.

**Solution of the boundary value problem.** Here, a solution methodology will be established for the displacement-based problem as stated in equation {8}. Per mechanical equilibrium, at any instant of time the virtual work form of the equilibrium equation in the absence of external loads can be given as:

$$\int_V \sigma^T \delta\varepsilon dV = 0 \quad \{14\}$$

where $V$ is the volume. Assuming the solution is known at time $t-\Delta t$, seeking solution at time $t$ via virtual work corresponds to:

$$\int_V \sigma(t)^T \delta(\varepsilon(t-\Delta t) + \Delta\varepsilon\big|_t) dV = \int_V \sigma(t)^T \delta(\Delta\varepsilon\big|_t) dV = 0 \quad \{15\}$$

Here $\delta\varepsilon(t\text{-}\Delta t)$ vanishes because the solution is known at time $t\text{-}\Delta t$. For $\sigma(t)$, equation {8} can be approximated via an explicit forward difference scheme in time:

$$\sigma^n \cong M_{n-1}^n \varepsilon^0 + \sum_{k=1}^n M_{k-1}^{n-(k-1)} \Delta\varepsilon^k \quad \{16\}$$

where:

$$\sigma^n = \sigma(n\Delta t),$$

$$M_{k-1}^{n-(k-1)} = M\left(\left(n-(k-1)\right)\Delta t, P\left((k-1)\Delta t\right)\right),$$

$$\Delta\varepsilon^k = \varepsilon^k - \varepsilon^{k-1}, k = 1,2,\cdots,n \text{ and } \varepsilon^0 = \varepsilon(0).$$

Using an isoparametric formulation (strain displacement matrix $B$ in {2} and {3}) developed in the winding section, substituting {16} into {15} and invoking the virtual work principle leads to discrete equations for an element:

$$\overline{K_e} \Delta u^n{}_e = F^n{}_e \quad \{17\}$$

where $\overline{K_e}$, $F^n{}_e$ and $\Delta u^n{}_e$ are the viscoelastic stiffness matrix, force vector and incremental displacements for element e, at time step *n, and:*

$$\overline{K_e} = \int_{-1}^{1}\int_{-1}^{1} B^T \left(M_{n-1}^1\right)_e B \det[J] r d\eta d\xi \quad \{18\}$$

$$F^n{}_e = -\int_{-1}^{1}\int_{-1}^{1} B^T \left(M_{n-1}^n \varepsilon^0 + \sum_{k=1}^{n-1} M_{k-1}^{n-(k-1)} \Delta\varepsilon^k\right) \det[J] r d\eta d\xi \quad \{19\}$$

$$\Delta\varepsilon^n{}_e = B \Delta u^n{}_e \quad \{20\}$$

*Conversion between stiffness and compliance tensors.* This solution is written in terms of the stiffness tensor $M$. Because the stiffness tensor and the compliance tensor are two representations of the same material properties, they are not independent from each other. $C$ and $M$ are related through the convolution relation {21}.

$$\int_0^t M(t,P) C(t-\tau,P) d\tau = tI \quad \{21\}$$

where $I$ is the fourth-order unit tensor and $t$ is time. This relation implies that the material can be characterized either via relaxation tests directly measuring the relaxation functions $E$ or via creep tests directly measuring the creep functions $J$. Because the model aims principally at modeling creep phenomena, the webs were characterized via creep tests, determining the compliance tensor. However, equilibrium equations are generally written in a displacement-based framework corresponding to equation {8}, meaning in terms of the stiffness tensor (equations {18} and {19}).

As pointed out by equation {21} and contrary to the elastic case, the stiffness tensor is not the inverse of the compliance tensor. An efficient discretization of the conversion developed by Baumgaertel [20] will be employed here to compute the stiffness tensor from the compliance tensor.

**Simplification of the compliance tensor.** A simplified compliance tensor $C$ with respect to the creep functions is proposed. The radial $J_r$ and tangential $J_\theta$ creep terms are defined as Prony series, following [9]:

$$J_r(t) = \frac{1}{E_r} + \sum_{i=1}^{m_r} \frac{J_{r,i}^*}{P}\left(1 - Exp\left[-\frac{t}{\lambda_{r,i}}\right]\right) \quad \{22\}$$

$$J_\theta(t) = \frac{1}{E_\theta} + \sum_{i=1}^{m_\theta} J_{\theta,i}\left(1 - Exp\left[-\frac{t}{\lambda_{\theta,i}}\right]\right) \quad \{23\}$$

where $J_{x,i}$ is the creep function and $\lambda_{x,i}$ the retardation time of the branch $I$ in the direction $x$. In addition, the transient part of the creep function is defined as $J_{r,trans}(t) = -\sum_{i=1}^{m_r} \frac{J_{r,i}^*}{P} Exp\left[-\frac{t}{\lambda_{r,i}}\right]$ and $J_{\theta,trans}(t) = -\sum_{i=1}^{m_r} J_{\theta,i} Exp\left[-\frac{t}{\lambda_{\theta,i}}\right]$.

Axisymmetric models also require the characterization of the axial creep function ($J_z$). Axisymmetric winding simulations [15] reveal that the behavior along the z direction has insignificant effects on the radial ($\sigma_r$) and tangential ($\sigma_\theta$) stress distribution but has a rather profound effect on shear ($\sigma_{rz}$) and axial ($\sigma_z$) stresses. To measure the creep compliance in the $z$ direction ($J_z$), the same characterization method used for $J_\theta$ can be employed and a Prony series can be fit. For the web materials used herein the in-plane elastic properties were essentially equal in the tangential and axial directions ($E_\theta \approx E_z$) and in this study the creep behavior in the plane of the web will be assumed to be isotropic ($J_z = J_\theta$). This assumption is reasonable for cast films and films that are drawn equivalently in the MD and CMD during orientation. The creep function $J_z$ will in general be different from $J_\theta$ for orthotropic films and will require separate characterization.

The shear behavior is assumed elastic, and the shear compliance $J_{rz}$ was set to $1/G_{rz}$ where $G_{rz}$ is the elastic shear modulus. There has been no documented attempt for the measurement of this value in viscoelastic regime for web materials. In another study, the authors found that $G_{rz}$ is pressure-dependent and for winding problems can be taken equal to $2E_r$ [22].

In this formulation, the coupled creep function terms are neglected by setting the off diagonal terms to zero (i.e. $J_{r\theta} = J_{\theta r} = J_{rz} = J_{zr} = 0$). This assumption has been deemed valid because parametric studies of axisymmetric winding models [7,15] show that the Poisson coupling terms in the elastic winding solution ($\nu_{r\theta}$ and $\nu_{\theta r}$) have a negligible impact on the residual winding stresses in rolls [9]. There have been no attempts to experimentally measure the coupled creep function terms for layers of web in stacks. Some experiments report that the elastic Poisson's ratio ($\nu_{r\theta}$) is state-dependent and small [21]. In the winding literature, the general assumption is that the out-of-plane Poisson's ratios ($\nu_{r\theta}$, $\nu_{rz}$) are small [9] and possibly state-dependent whereas the in-plane Poisson's ratio ($\nu_{z\theta}$) is constant and ranges from 0.3 to 0.4. Consequently, in this study, the coupled creep function terms ($J_{r\theta}$ *and* $J_{\theta r}$) will be assumed to be negligible in comparison to the uncoupled terms ($J_r$ *and* $J_\theta$). This assumption effectively decouples the viscoelastic behavior in the different directions.

In summary, a simplified decoupled viscoelastic compliance tensor has been obtained:

$$\bar{C}(t,P)=\begin{bmatrix} J_r(t,P) & 0 & 0 & 0 \\ 0 & J_z(t) & 0 & 0 \\ 0 & 0 & 1/G_{rz} & 0 \\ 0 & 0 & 0 & J_\theta(t) \end{bmatrix} \quad \{24\}$$

**Expressions of the stress and strain tensors.** This formulation also decouples the nonlinear (pressure-dependent) and linear terms. A solution is proposed for the general nonlinear creep behavior in the radial direction whether the transient part is state-dependent or not and without relying on the conversion of radial creep functions. The method is based on the observation that the viscoelastic behavior of the web in the wound rolls results from two fundamental mechanisms: the first is the tangential relaxation of the layer under tensile stresses in the circumferential direction and the second is the creep of the layer under radial pressure, as seen in Figure 3. These two processes are combined in a unique way, which employs direct usage of radial creep function $J_r$.

The radial creep results in radial strain. At a given time $t$, the total radial creep strain can be calculated from the transient portion of the radial creep function:

$$\varepsilon_{r,creep}(t) = J_{r,trans}(t)\sigma_r(0) + \int_0^t J_{r,trans}(t-\tau)\frac{\partial \sigma_r}{\partial \tau}d\tau \quad \{25\}$$

This creep causes a radial deformation which can be calculated via the strain displacement relation:

$$\varepsilon_{r,creep}(t) = \frac{du_{r,creep}}{dr} \rightarrow u_{r,creep}(t) = \int_{r_c}^{r} \varepsilon_{r',creep}(t)dr' \quad \{26\}$$

where $r$ is the radius at which the layer is located and $r_c$ is the outer radius of the core of the roll.

This radial strain can be incorporated as a tangential strain in addition to the actual tangential strain:

$$\frac{u_{r,creep}}{r} = \bar{\varepsilon_\theta}(t) \quad \{27\}$$

The tangential stress becomes:

$$\sigma_\theta(t) = \left(\varepsilon_\theta(0) + \bar{\varepsilon_\theta}(t)\right)E_\theta(t) + \int_0^t E_\theta(t-\tau)\frac{\partial \varepsilon_\theta}{\partial \tau}d\tau \quad \{28\}$$

Thus, the viscoelastic effects on the tangential stress are combined. The tangential stress and strain result from tension in the web as it enters the wound roll and are significantly larger than the stress imposed in other directions. Consequently, the effect of the tangential stress dominates the mechanical response of a wound roll.

**Explicit forward difference scheme.** An explicit forward difference scheme can be developed for equation {25}:

$$\varepsilon_{r,creep}{}^n = \sigma_r{}^{n-1}\sum_{i=1}^{m_r} J_{r,i} - \sigma_r{}^0\sum_{i=1}^{m_r} J_{r,i}Exp\left[-\frac{n\Delta t}{\lambda_{r,i}}\right] - \sum_{i=1}^{m_r} J_{r,i}H_{r,i}{}^n + \Delta\sigma_r{}^n\sum_{i=1}^{m_r} J_{r,i} \quad \{29\}$$

where

$$\sigma_r{}^n = \sigma_r{}^{n-1} + \Delta\sigma_r{}^n \text{ with } \sigma_r{}^0 = \sigma_r(0)$$

$$H_{r,i}{}^n = \left(H_{r,i}{}^{n-1} + \Delta\sigma_r{}^{n-1}\right) Exp[-\Delta t/\lambda_{r,i}] \text{ with } H_{r,i}{}^0 = 0$$

$H_{r,i}{}^n$ is the hereditary portion and the exponential formulation is particularly convenient because there is no need to store the entire solution history [9]. The integral in equation {26} is approximated by a finite sum via the rectangular numerical integration method:

$$u_{r,creep}{}^n = \int_{r_c}^{r} \varepsilon_{r',creep}{}^n dr' \cong h \sum_j \varepsilon_{r_j,creep}{}^n \quad \{30\}$$

where $r_j$ denotes radial positions of equally spaced sectors (with sector thickness $h$) along the radial direction from the core outer radius ($r_c$) to a radius of interest $r$ in the roll. The natural layer-wise structure of the wound roll is utilized in the calculation of {30}. Hence $h$ is the average model layer thickness and $\varepsilon_{r_j,creep}{}^n$ is the radial creep calculated at layer $j$. Consequently, $j$ runs from *1* to $k$ when calculating the total radial deformation for the $k^{th}$ layer. The corresponding tangential strain can be determined from equation {27} and used in a discrete form of equation {28}:

$$\sigma_\theta{}^n = (\varepsilon_\theta{}^{n-1} + \bar{\varepsilon}_\theta{}^n) E_{\theta,\infty} - (\varepsilon_\theta{}^0 + \bar{\varepsilon}_\theta{}^n) \sum_{i=1}^{m_\theta} E_{\theta,i} Exp\left[-\frac{n\Delta t}{\tau_{\theta,i}}\right] - \sum_{i=1}^{m_\theta} E_{\theta,i} G_{\theta.i}{}^n + E_{\theta,0} \Delta\varepsilon_\theta{}^n \quad \{31\}$$

where:

$$\varepsilon_\theta{}^n = \varepsilon_\theta{}^{n-1} + \Delta\varepsilon_\theta{}^n \text{ with } \varepsilon_\theta{}^0 = 0$$

$$G_{\theta,i}{}^n = \left(G_{\theta,i}{}^{n-1} + \Delta\varepsilon_\theta{}^{n-1}\right) Exp[-\Delta t/\tau_{\theta,i}] \text{ with } G_{\theta,i}{}^0 = 0$$

$$E_\infty = E_0 + \sum_{i=1}^{m} E_i$$

$G_{\theta,i}{}^n$ is the hereditary component carrying the history of the deformation during the tangential relaxation. A similar expression for the axial (z) direction can be developed:

$$\sigma_z{}^n = (\varepsilon_z{}^{n-1}) E_{z,\infty} - (\varepsilon_z{}^0) \sum_{i=1}^{m_z} E_{z,i} Exp\left[-\frac{n\Delta t}{\tau_{z,i}}\right] - \sum_{i=1}^{m_z} E_{z,i} G_{z.i}{}^n + E_{z,0} \Delta\varepsilon_z{}^n \quad \{32\}$$

A finite element model can be developed with the time-dependent stress components, as the virtual work at time $n$ can be given as:

$$\int_V \left(\sigma^n\right)^T \delta\Delta\varepsilon^n dV = 0 \quad \{33\}$$

This leads to the finite element stiffness equation for a typical element e:

$$\overline{K_e} \Delta u^n{}_e = F^n{}_e \quad \{34\}$$

$$\overline{K_e} = \int_{-1}^{1}\int_{-1}^{1} B^T \left(\overline{M}_{n-1}^0\right)_e B det[J] r d\eta d\xi \quad \{35\}$$

$$F^n{}_e = -\int_{-1}^{1}\int_{-1}^{1} B^T\left(A^n\right) det\left[J\right] r d\eta d\xi \qquad \{36\}$$

Here, $\overline{\overline{M}}^0_{n-1}$ is the reduced stiffness tensor corresponding to the inverse of the reduced compliance matrix $\bar{C}$ in {25} at time t=0:

$$\overline{\overline{M}}^0_{n-1} = \overline{\overline{M}}(0, \sigma_r^{n-1}) = \begin{bmatrix} E_r^{n-1} & 0 & 0 & 0 \\ 0 & E_z & 0 & 0 \\ 0 & 0 & 2E_r^{n-1} & 0 \\ 0 & 0 & 0 & E_\theta \end{bmatrix} \qquad \{37\}$$

The tensor $A^n$ is the residual stress tensor for step $n$ and is given as:

$$A^n = \begin{bmatrix} \sigma_r^{n-1} \\ \left(\varepsilon_z^{n-1}\right) E_{z,\infty} - \left(\varepsilon_z^0\right) \sum_{i=1}^{m_z} E_{z,i} Exp[-\frac{n\Delta t}{\tau_{z,i}}] - \sum_{i=1}^{m_z} E_{z,i} G_{z,i}^n \\ \sigma_{rz}^{n-1} \\ \left(\varepsilon_\theta^{n-1} + \overline{\varepsilon_\theta}^n\right) E_{\theta,\infty} - \left(\varepsilon_\theta^0 + \overline{\varepsilon_\theta}^n\right) \sum_{i=1}^{m_\theta} E_{\theta,i} Exp[-\frac{n\Delta t}{\tau_{\theta,i}}] - \sum_{i=1}^{m_\theta} E_{\theta,i} G_{\theta,i}^n \end{bmatrix} \qquad \{38\}$$

| process # | Description |
|---|---|
| 1 | input geometrical and material data |
| 2 | use winding algorithm to obtain initial stresses $\sigma_{rz}{}^0$ $\sigma_r{}^0$ and strains $\varepsilon_\theta{}^0$ , $\varepsilon_z{}^0$ |
| 3 | convert tangential and axial creep functions to relaxation functions |
| 4 | set initial conditions time step $n=1$, $E_r{}^0=K_2(-\sigma_r{}^0+K_1)$, $H_{r,i}{}^0=G_{\theta,i}{}^0=G_{z,i}{}^0=0$ |
| 5 | start time step $n$ |
| 5.1 | form stiffness matrix for all elements per equation {35}, using the material matrix {37}) at t=0 |
| 5.2 | calculate radial creep for all elements per equation {29}: since $\Delta\sigma_r{}^n$ is not known currently, use extrapolated value from two previous steps $\Delta\sigma_r{}^n \approx 2\Delta\sigma_r{}^{n-1} - \Delta\sigma_r{}^{n-2}$ |
| 5.3 | calculate components $A_\theta{}^n$ and $A_z{}^n$ per {38} |
| 5.4 | form force vector for all elements per {36} |
| 5.5 | assemble and solve system of equations {34}, obtain incremental displacements $\Delta u^n$, calculate incremental strains $\Delta\varepsilon^n$ *and stresses* $\Delta\sigma^n = M_{n-1}{}^0\Delta\varepsilon_n$ |
| 5.6 | calculate current stresses $\sigma^n = A^n + \Delta\sigma^n$ |

| | |
|---|---|
| 5.7 | Has the target time $t$ been achieved? ($n\Delta t \geq t$)<br>**if <u>NO</u>** then set $n=n+1$ calculate $H_{r,i}^{n}$, $G_{\theta,i}^{n}$, $G_{z,i}^{n}$ and<br>$E_r^{n-1}=K_2(-\sigma_r^{n-1}+K_1)$ *go to process 5* ***else*** *go to process 6* |
| 6 | print results (stresses and strains for time $t$) |

Table 1 – Flow Chart for Phase II Solution

The core section that the roll is wound upon is considered to be elastic and contributes to the system elastically only via the elastic stiffness tensor. The steps of the algorithm for the viscoelastic model are given in Table 1.

This concludes the development of the second phase of the analysis. This development allows the determination of the stresses, strains and length changes due to creep during storage as a result of the residual stresses and strains created by winding,

## CHARACTERIZATION OF WEB MATERIALS

As examples of viscoelastic webs, we studied a low-density polyethylene web[1] (LDPE) and a spunbond-meltblown-spunbond[2] (SMS) nonwoven. These webs creep readily at room temperature and were good candidates to explore length changes due to creep in roll storage. In order to simulate the behavior of these webs in storage, we first need to fully characterize their viscoelastic properties.

### Geometry of the Web and Instantaneous Properties

The web thickness was measured at minimal pressure by creating stacks of web, measuring the stack height and dividing by the number of web layers. The MD modulus was inferred from manual load-deformation tests on specimens 25.4 cm long and 2.54 cm wide, where the strain rate was limited by data recording at 10%/min. The radial modulus is measured through a compression stack test at a relatively high strain rate. The Pfeiffer's coefficients [18] are fitted on the resulting stress-strain curve. The Poisson's ratios are estimated according to the discussion above. The elastic properties of the core are also measured as the first layers of the model will be core layers (Figure 2).

| | | SMS | LDPE |
|---|---|---|---|
| Web thickness | | 0.119 mm (0.0047 in) | 0.508 mm (0.02 in) |
| Web width | | 19.1 cm (7.5 in) | 10.2 cm (4 in) |
| MD modulus | | 106 MPa (15425 psi) | 144 MPa (21000 psi) |
| $\nu_{rz}$, $\nu_{r\theta}$ | | 0 | 0 |
| $\nu_{z\theta}$ | | 0.3 | 0.3 |
| Radial modulus | $K_1$ | 758 Pa (0.11 psi) | 0 Pa (0.0 psi) |
| | $K_2$ | 12.985 | 246.5 |
| Core modulus | | 3.45 GPa (500 ksi) | 207 GPa (30 Mpsi) |
| Core Poisson ratio | | 0.3 | 0.3 |

Table 2 – Elastic and geometric web properties

### Tangential Viscoelastic Properties

[1] Blueridge Films, 10921 Lamore Drive, Disputanta, VA 23842
[2] Kimberly-Clark Corporation, 351 Phelps Drive Irving, Texas 75038, USA

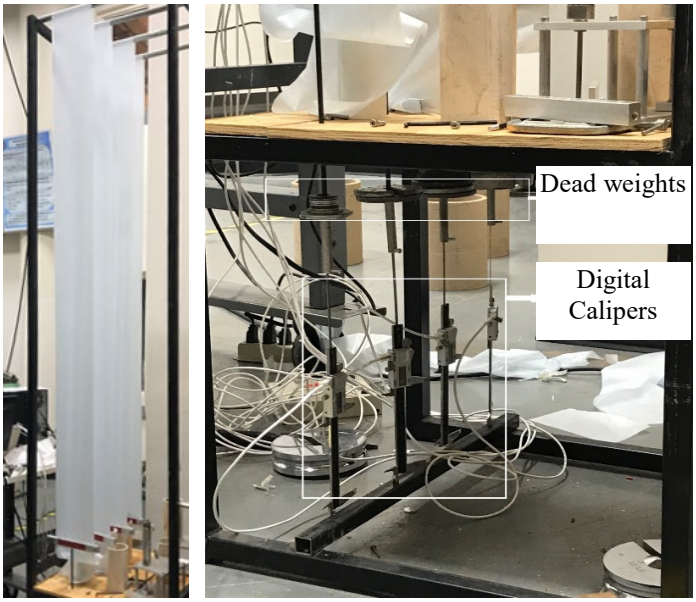


Figure 4 – Characterization Apparatus for MD Creep

The MD creep of the webs was characterized in the apparatus shown in Figure 4. Several SMS and LDPE web specimens of length 2.1 m (85 in) were subjected to constant loads using dead weights (10, 15, and 20 lb). The samples were stress free except for that induced by their own weight until testing began. The clamps and weights were then lowered and calipers[3] with digital output were used to record the displacements of the samples through time. The recorded displacements were divided by the unstressed specimen length to obtain the strain. This strain had both instantaneous elastic and transient viscoelastic components. The instantaneous strain was estimated as the stress divided by the MD modulus (Table 2). The instantaneous strains were then subtracted from the measured strains to obtain the transient strains. The transient strains were normalized by dividing by the applied stress levels and are shown in Figure 5 for the SMS. Finally, the normalized strains corresponding to the various stress levels were average and a Prony series expression (equation {39}) similar to the transient portion of {23} was fit to the curve. The coefficients of the obtained Prony series for the creep function are presented in Table 3.

$$J_{\theta,trans}(t) = J_{\theta,0} + J_{\theta,1}e^{\left(-t/\lambda_{\theta,1}\right)} + J_{\theta,2}e^{\left(-t/\lambda_{\theta,2}\right)} + J_{\theta,3}e^{\left(-t/\lambda_{\theta,3}\right)} + J_{\theta,4}e^{\left(-t/\lambda_{\theta,4}\right)} \quad \{39\}$$

where $J_{\theta,0} = -(J_{\theta,1} + J_{\theta,2} + J_{\theta,3} + J_{\theta,4})$.

[3] AccuRemote, 1301 Calle Avanzado, San Clemente, CA 92673, USA

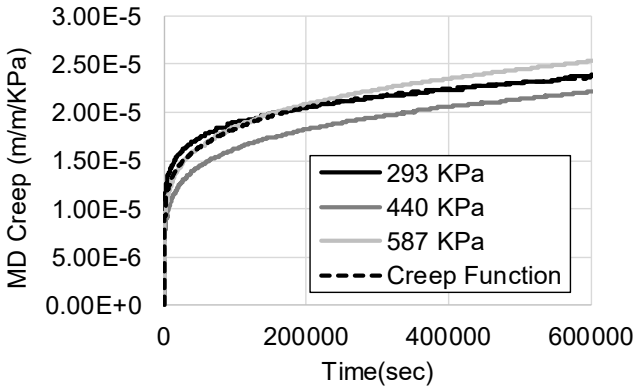


Figure 5 – Normalized MD Creep of SMS at 21ºC (70ºF)

| | SMS | LDPE |
|---|---|---|
| $J_{\theta,0}$ (m/m/KPa) | 4.5E-05 | 5.11E-06 |
| $J_{\theta,1}$ (m/m/KPa) | -2.0E-05 | -2.71E-06 |
| $J_{\theta,2}$ (m/m/KPa) | -5E-06 | -9.09E-08 |
| $J_{\theta,3}$ (m/m/KPa) | -5E-06 | -6.76E-07 |
| $J_{\theta,4}$ (m/m/KPa) | -1.5E-05 | -1.64E-06 |
| $\lambda_{\theta,1}$ (s) | 100 | 1,000 |
| $\lambda_{\theta,2}$ (s) | 10,000 | 10,000 |
| $\lambda_{\theta,3}$ (s) | 100,000 | 100,000 |
| $\lambda_{\theta,4}$ (s) | 1,000,000 | 1,000,000 |

Table 3 – MD creep Prony transient terms for SMS and LDPE webs at room temperature

**Radial Viscoelastic Properties**

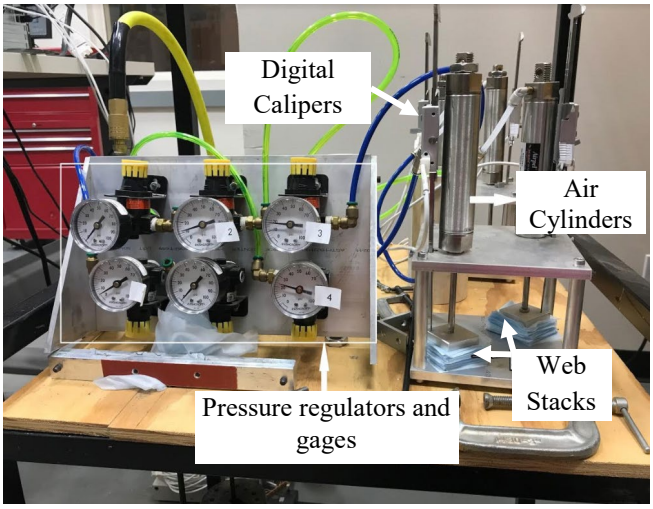


Figure 6 – Characterization Apparatus for Radial Creep

The radial creep of the webs was characterized in the apparatus shown in Figure 6. Stacks of SMS and LDPE web were compressed using air cylinders whose unique pressures were controlled by the regulators shown. The pressure within the air cylinder induced a compressive force on the platen that compressed the stack at a constant pressure through time. Calipers with digital output were used to measure the displacement of the web stacks which were recorded through time[3]. The total strain was obtained by dividing by the uncompressed stack height. The instantaneous strain was calculated by providing the known stack pressure $P$ and values of $K_1$ and $K_2$ to expression {5} and solving for $\varepsilon_r$. The transient radial strains were obtained by subtracting the instantaneous elastic strains from the total measured strains. The transient viscoelastic strains were normalized by dividing by the applied pressure. Normalized radial creep data for the SMS web is presented in Figure 7. The creep function of $J_{r,trans}(t)$, similar to expression {39}, was fit to the average creep data and the Prony series coefficients are provided in Table 4 for SMS and LDPE webs.

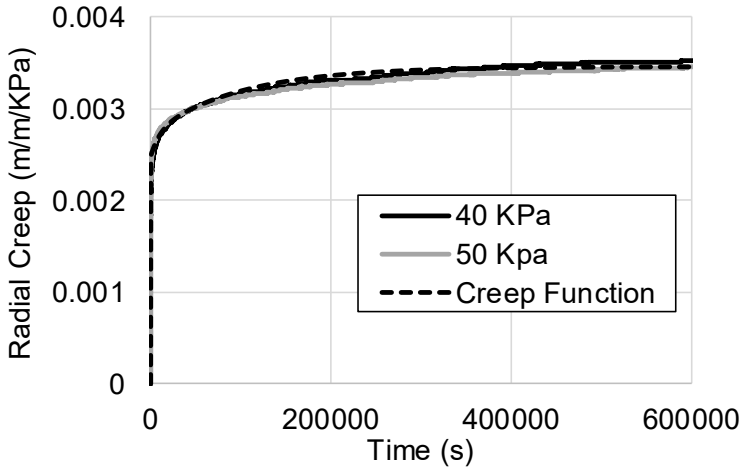


Figure 7 – Radial Creep of SMS at 21°C (70°F)

| | SMS | LDPE |
|---|---|---|
| $J_{r,0}$ (m/m/KPa) | 0.00346 | 2.64E-06 |
| $J_{r,1}$ (m/m/KPa) | -0.00248 | -1.29E-06 |
| $J_{r,2}$ (m/m/KPa) | -0.00026 | -1.35E-06 |
| $J_{r,3}$ (m/m/KPa) | -0.00072 | |
| $\lambda_{r,1}$ (s) | 100 s | 696 s |
| $\lambda_{r,2}$ (s) | 10,000 s | 72,810 s |
| $\lambda_{r,3}$ (s) | 100,000 s | |

Table 4 – Radial creep Prony transient terms for SMS and LDPE webs at room temperature

## RESULTS

The webs studied had no known thickness variation across the width and thus a 2D axisymmetric winding model is not needed for these simulations. Therefore, the 2D

model will be constrained to one sector with constant web thickness, essentially a 1D simplification. The material parameters in Tables 2-4 were input for each specific web. The model is setup to wind the web on a core to a finish radius input by the user. The winding model input parameters are provided in Table 5.

| | SMS | LDPE |
|---|---|---|
| Core inner radius | 8.57 cm (3.375 in) | 3.81 cm (1.5 in) |
| Core outer radius ($r_c$) | 9.84 cm (3.875 in) | 4.44 cm (1.75 in) |
| Roll outer radius ($r_{out}$) | 10.7 cm (4.21 in) | 10.4 cm (4.11 in) |
| Winding Tension Stress | 587 KPa (85.1 psi) | 1.38 MPa (200 psi) |
| Roll Storage Time | 4 days | 7 days |

Table 5 – Winding Input Parameters

There is considerable winding residual stress decrease in these rolls due to viscoelasticity. For the SMS web, substantial decreases in radial pressure and tangential stress are seen after 4 days of storage (Figure 9). A similar behavior is witnessed for the LDPE web for 7 days of storage (Figure 10). The tangential viscoelastic strains for both the SMS and LDPE webs are shown to begin from near zero at the core and increase monotonically with increasing wound roll radius (Figure 11). These strains are small near the core since the core material is assumed to be elastic and exhibits a large modulus compared to that of the web (Table 2). In these examples, the web layers near the core are behaving much like a material subjected to simple stress relaxation. The tangential strain within the web is constrained by a large core stiffness while the tangential stress near the core decreases (Figures 9 and 10). The web layers close to the outer radius of the roll are subject to a large tangential stress and no radial pressure. Consequently, a relatively high tangential creep strain is measured for these layers.

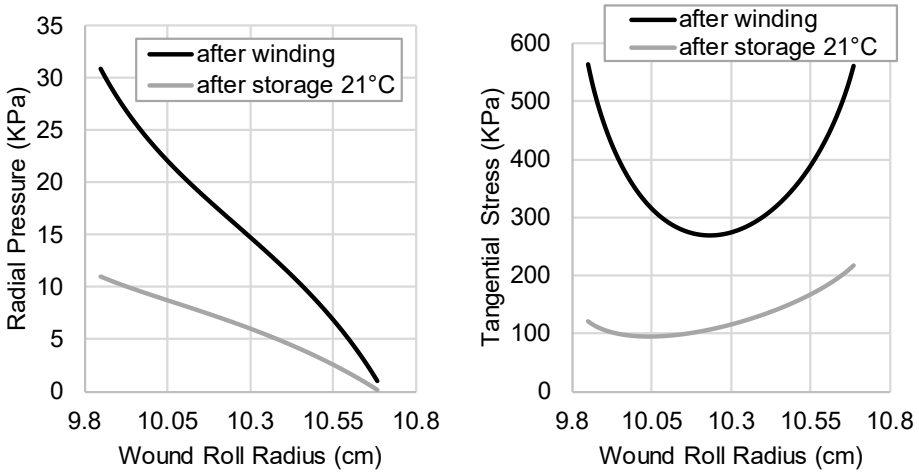


Figure 9 – Residual stresses in SMS after winding and after 4 days storage

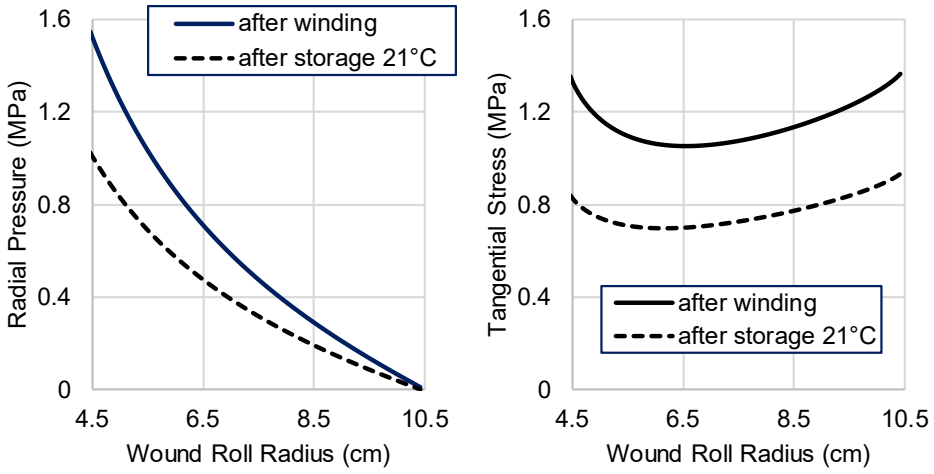


Figure 10 – Residual stresses in LDPE after winding and after 7 days storage at 21°C.

The total change in web length due to creep can be predicted from the tangential viscoelastic strains using the following expression:

$$\Delta L = \int_{r_c}^{r_{out}} 2\pi r \varepsilon_{vt} dr \qquad \{40\}$$

where $\varepsilon_{vt}$ is the viscoelastic tangential strain (Figure 11).

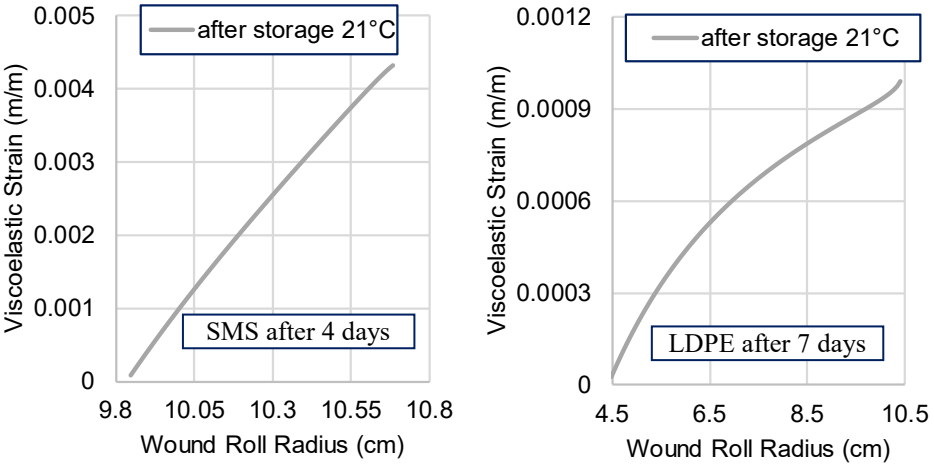


Figure 11 – Tangential viscoelastic strains in SMS and LDPE after storage

## COMPARISON WITH WINDING EXPERIMENTS

To conduct winding trials, three samples of SMS and LDPE web were cut in excess of 45.7 m (1800 in) length and 54.9 m (2160 in) length, respectively. The samples were

allowed to relax at no tension for several days in a hallway (Figure 8). Marks were made across the SMS and LDPE web width at a length interval of 45.7 m and 54.9 m, respectively. The webs were carefully coiled on a core by hand with little tension.

The SMS coiled web was then unwound and rewound in a web line equipped with a photodiode[4] and a Laser Doppler Velocimeter[5] (Figure 8) at a tensile stress of 587 KPa (85.1 psi), corresponding to a web tension of 13.3 N (3 lb). When the first mark passed the photodiode, a counter was triggered and began counting pulses. These pulses were proportional to the deformed length output by the Laser Doppler Velocimeter. When the second mark passed the photodiode, the counter was triggered off and the total deformed length of the rewound web was known. The winding of 45.7 m of web was completed quickly and it was assumed the web deformed length was due to elastic behavior. The roll was then stored for 4 days at room temperature (21ºC). The roll was then unwound on the web line and again the deformed length between the two marks was measured. The difference in the deformed length of web wound off of the roll minus the deformed length wound in was assumed to be a measure of the increased web length due to creep during the 4-day storage period. This test was repeated three times with new web samples.

The LDPE web was to be wound at a tensile stress of 1.38 MPa (200 psi), corresponding to a web tension of 71.1 N (16 lb), This required the use of a second web line able to develop that tension. The photodiode/LDV measurement system was not available on that web line. Nonetheless, the three LDPE rolls were wound and stored for 7 days at room temperature. The webs were then quickly unwound in the hallway and the distance between the two marks was measured with a steel rule. The difference between the measured lengths before and after storage in a wound roll were assumed to be the web length increase due to viscoelastic creep.

The test results are shown in Table 6. On average, SMS web length increased by 12.6 cm during the 4-day storage period and the LDPE web length increased by 4.3 cm during the 7-day storage period. In both cases, the standard error is below 2.5% of the mean, which was deemed acceptable.

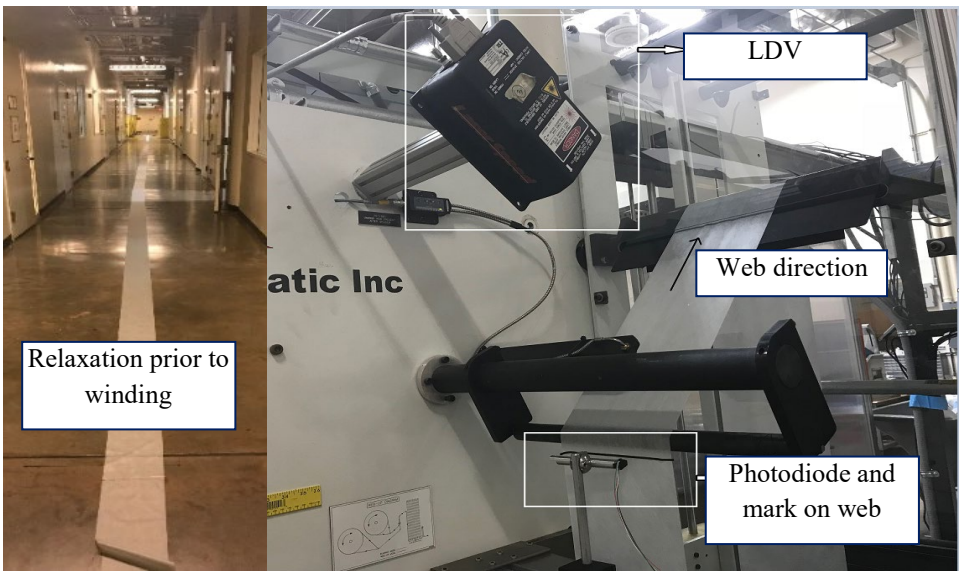


Figure 8 – Experimental Setup for SMS winding creep tests

| Web | Winding tension (KPa) | Storage time (days) | Storage temperature (°C) | Web Length (m) | Increased web length (cm) | | | | |
|---|---|---|---|---|---|---|---|---|---|
| | | | | | Test 1 (cm) | Test 2 (cm) | Test 3 (cm) | Test average (cm) | Standard Error (cm) |
| SMS | 587 | 4 | 21 | 45.7 | 13.2 | 12.3 | 12.2 | 12.6 | 0.31 |
| LDPE | 1380 | 7 | 21 | 54.9 | 4.3 | 4.3 | 4.4 | 4.3 | 0.05 |

Table 6 – Increased web length due to viscoelasticity

Finally, the winding experimental results can be compared to the model, as presented in Table 7.

| Web | Winding tension (KPa) | Storage time (days) | Storage temperature (°C) | Web Length (m) | Increased web length (cm) | | |
|---|---|---|---|---|---|---|---|
| | | | | | Test average | Model | %Error |
| SMS | 587 | 4 | 21 | 45.7 | 12.6 | 10.8 | 14.3 |
| LDPE | 1380 | 7 | 21 | 54.9 | 4.3 | 3.7 | 14.0 |

Table 7 – Comparison of experiments and model web length increase during to storage.

The predictions of the model compared very well with the corresponding experiments, showing an error of about 14% for both the SMS and the LDPE web (Table 7). Considering the large differences between these webs in terms of winding tension, storage time, material behavior, and viscoelastic time scales, this result is remarkable.

To put these viscoelastic deformations in context, consider what web length increase would have occurred in these materials had they not been wound into rolls but subject to the same winding stress. Often the residual stresses due to winding are considered a bane in terms of wound roll defects. We estimate the creep due to the winding stress in the CMD direction using the creep function in Table 3. The results are presented in Table 8. Comparing Tables 7 and 8 shows the creep strain in the wound roll are 10 to 12% what they would have been if the web was stored as strips under tension. This speaks to the benefit of winding webs into rolls, in addition to the obvious gain in space.

| Web | Web tension (KPa) | Storage time (days) | Storage temperature (°C) | Web Length (m) | Increased web length (cm) |
|---|---|---|---|---|---|
| SMS | 587 | 4 | 21 | 45.7 | 91.8 |
| LDPE | 1380 | 7 | 21 | 54.9 | 31.9 |

Table 8 – Length increase of web subjected to constant MD stress

## CASE STUDY: INDUCING CAMBER INTO AN LDPE WEB

To demonstrate the benefit of the time-dependent winding model presented here, the origin of the web camber defect is proven. Web camber has been shown to induce lateral CMD tracking errors in webs. Several studies have shown the web will continually track toward the longer web edge [23-25]. The 2D version of the winding model demonstrates the source of web camber.

Consider a case where the LDPE web, 10.2 cm wide and nominally 0.508 mm thick (Table 1), has a thickness variation over the width, which persists in the MD. The web thickness will be assumed to vary linearly from 0.513 mm at CMD location -5.1 cm (left edge) to 0.503 mm at CMD location 5.1 cm (right edge). A 54.9 m length of the LDPE web will be wound onto the core defined in Table 6. The average winding tensile stress will remain 1380 KPa. The profile of the deformed outer radius is shown in Figure 12 as a function of wound roll radius. Because of the thickness variation, the winding roll now takes the shape of a truncated cone. Near the core, the wound roll is nearly of cylindrical shape but as additional layers with their thickness variation are wound on, the roll is 1.09 mm larger at the left edge than at the right edge. The core of the wound roll has one unique angular velocity $\omega$. Thus, greater linear MD velocity ($V=r\omega$) is expected at the left edge of the roll than the right edge and coincidentally greater MD $\sigma_\theta$ stress will be expected on the left versus right edge of the web when it is wound onto the roll (Figure 13).

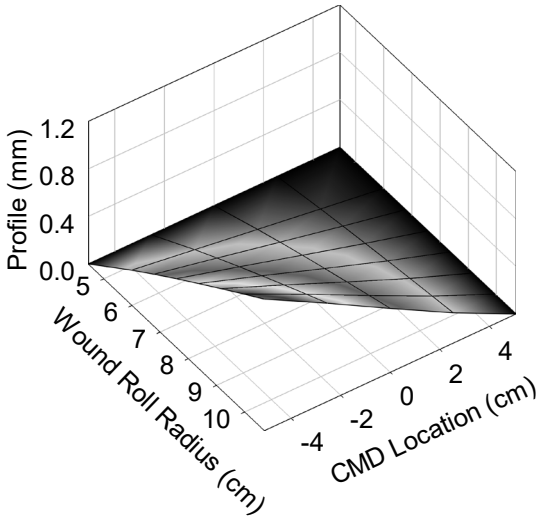


Figure 12 – Radius variation versus web width as a function of wound roll radius.

The tangential stress is 1352 KPa at the widthwise center of the web (CMD location 0 cm) at the outside of the wound roll (radius=10.4 cm) just after winding. The tangential stresses become largest at the left edge and smallest at the right edge of the outer layer. Also shown are the tangential stresses after 7 days of storage at room temperature (21°C), which are appreciably less than the stresses just after winding.

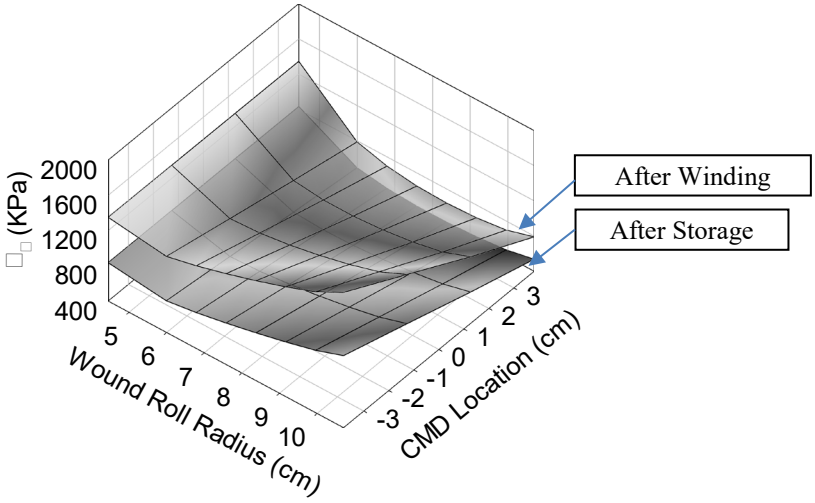


Figure 13 – LDPE tangential stresses for a web wound with variable thickness

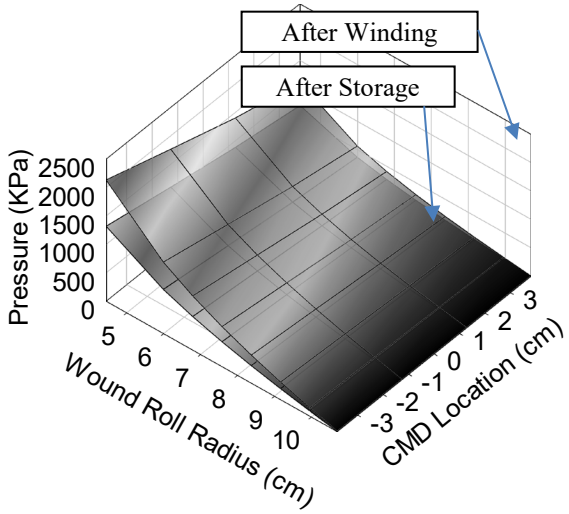


Figure 14 – LDPE radial pressures for a web wound with variable thickness

The radial pressures throughout the wound roll are shown in Figure 14 immediately after winding and after 7 days of storage. The spatial variation due to the thickness variation is appreciable. The radial pressure and tangential stress both contribute to the tangential strains.

The source of web camber is the MD viscoelastic strains seen in Figure 15. The average of these strains over the web width is very close to the strain for the constant thickness LDPE (Figure 11). Subtracting the average strains from the viscoelastic strains (Figure 15) leads to the bending strain $\varepsilon_b$. The bending strain is related to a stress-free web camber $\rho$ where $\rho$=y/$\varepsilon_b$ and y is the CMD location of the bending strain.

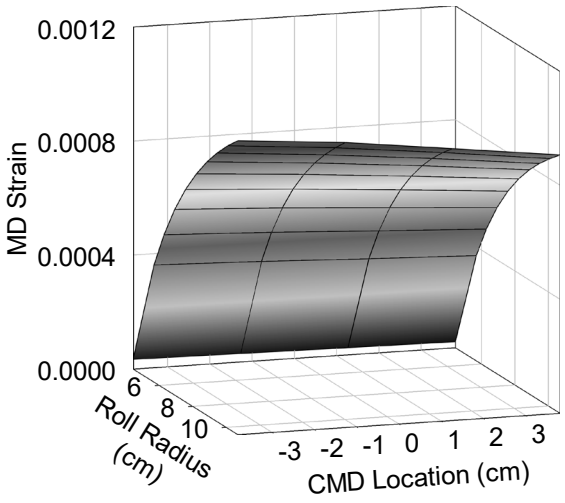


Figure 15 – Viscoelastic MD strain after 7 days of storage

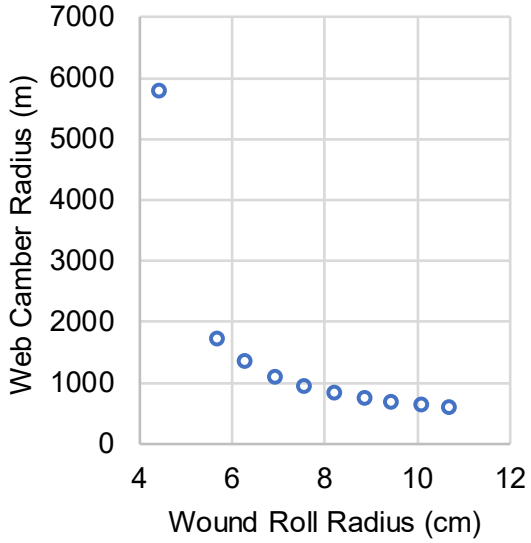


Figure 16 – Camber Radius of Unstressed Web

Thus, the unstressed camber radius can be predicted as a function of the radial position of the web layer in the wound roll (Figure 16). Dealing with lateral deformation and registration of webs in free spans is made more difficult with webs of variable camber being unwound into a web process machine. Webs will never be perfectly uniform in thickness but winding algorithms such as those presented herein can be used to predict what web thickness variation can be accepted based upon the viscoelastic characterization of the web and what camber radius is acceptable within the web.

## CONCLUSION

A deformation-based winding model has been developed, where the winding process is assumed entirely elastic and the storage in a wound roll viscoelastic. The model allows registration errors and other length defects due to viscoelastic relaxation of the web to be explored. Such a model is useful for studying winding parameters, storage conditions and web thickness variation that is acceptable with regard to registration error or camber in roll-to-roll processes. As an example, the model demonstrates how thickness variation in the width of the web results in web camber.

## ACKNOWLEDGEMENTS

The authors would like to thank the sponsors of the Web Handling Research Center of Oklahoma State University for supporting the research that made this publication possible.

## REFERENCES

1. Smith, R. D., Roll and Web Defect Terminology, 2nd edition, TAPPI Press, 2007.
2. Gajjalla, A., Markum, R., and Good, J.K., "Predicting the Web Length and Layers in a Wound Roll," Proceedings of the 15th International Conference on Web Handling, Stillwater, OK, June 10-13, 2019.
3. Hakiel, Z., "Nonlinear Model for Wound Roll Stresses," TAPPI J., Vol. 70, No. 5, May 1987, pp. 113-117.
4. Willett, M. S., and Poesch, W.L., "Determining the Stress Distribution in Wound Reels of Magnetic Tape using Nonlinear Finite Difference Approach," ASME J. Appl. Mech., Vol. 55, June 1988, pp. 365-371.
5. Good, J. K., Pfeiffer, J. D., and Giachetto, R. M., "Losses in Wound-on Tension in the Center Winding of Wound Rolls," Web Handling-1992, AMD-149, ASME, New York, 1992, pp. 1-11.
6. Benson, R. C., "A Nonlinear Wound Roll Model Allowing for Large Deformation," ASME J. Appl. Mech., Vol. 62, 1995, pp.853-859.
7. Mollamahmutoglu, C., and Good, J. K., "Analysis of Large Deformation Wound Roll Models," ASME J. Appl. Mech., Vol. 80, July 2013, pp. 041016-1-11.
8. Lin, J. Y., and Westmann, R. A., "Viscoelastic Winding Mechanics," ASME J. Appl. Mech., Vol. 56, No. 4, 1989, pp. 821-827.
9. Qualls, W. R., and Good, J. K., "Viscoelasticity in Wound Rolls," ASME J. Appl. Mech., Vol. 64, No. 1, March 1997, pp. 201-208.
10. Good, J. K., and Roisum, D. R., Winding: Machines, Mechanics and Measurements, TAPPI Press, Norcross, GA, 2008, pp. 239-250.
11. Acton, K., and Weick, B., "Viscoelastic Behavior of Polymer Tape in a Wound Roll," J. Appl. Polymer Sci., Vol. 122, No. 5, 2011, pp. 2884-2898.
12. Cole, K. A., and Hakiel, Z., "A Nonlinear Wound Roll Model Accounting for Widthwise Web Thickness Nonuniformities," Proceedings of the Web Handling Symposium, ASME Applied Mechanics Division, Vol. 149, 1992, pp. 13-24.
13. Lee, Y. M., and Wickert, J. A., "Stress Field in Finite Width Axisymmetric Wound Rolls," ASME J. Appl. Mech., Vol. 69, No. 2, 2002, pp. 130–138.
14. Hoffecker, P., and Good, J. K., "Tension Allocation in a Three Dimensional Wound Roll," Proceedings of the 8th International Conference on Web Handling, Web

Handling Research Center, Oklahoma State University, Stillwater, Oklahoma, 2005, pp. 565–581.
15. Arola, K., and von Hertzen, R., "Two Dimensional Axisymmetric Winding Model for Finite Deformation," Computational Mechanics, Vol. 40, No. 6, 2007, pp. 933–947.
16. Mollamahmutoglu, C., and Good, J. K., "Modeling the Influence of Web Thickness and Length Imperfections Resulting from Manufacturing Processes on Wound Roll Stresses," CIRP Journal of Manufacturing Science and Technology, Vol. 8, January 2015, pp. 22-33.
17. Good, J. K., Mollamahmutoglu, C., Markum, R., and Gale, J. W., "Residual Winding Stresses Due to Spatial Web Thickness Variation," ASME J. Manufacturing Science and Engineering, Vol. 139, No. 3, March 2017.
18. Pfeiffer, J. D., "Measurement of the K2 Factor for Paper," TAPPI J., Vol. 64, No. 4, 1981, pp. 105–106.
19. Ferry, J. D., Viscoelastic Properties of Polymers, Wiley, New York, 1961.
20. Baumgaertel, M., and Winter, H. H., "Determination of Discrete Relaxation and Retardation Time Spectra from Dynamic Mechanical Data," Rheologica Acta, Vol. 28, 1989, pp. 511-519.
21. Good, J. K., "Winding and Unwinding Webs: A Review of the State of the Science in 2005, Advances in Paper Science and Technology: Transactions of the 13th Fundamental Research Symposium," Editor: IAnson, SJ, Cambridge, UK, 2005, pp. 307-406.
22. Mollamahmutoglu, C., Ganapathi, S., and Good, J.K., "Pressures on Webs in Wound Rolls due to Winding and Contact," TAPPI J., 13 (2), pp. 41-50, 2014.
23. Shelton, J. J., "Effects of Web Camber on Handling," Proceedings of the 4th International Conference on Web Handling, Web Handling Research Center, Stillwater, Oklahoma, June, 1997, pp. 248-263.
24. Swanson, R. P., "Mechanics of Non-Uniform Webs," Proceedings of the 5th International Conference on Web Handling, Web Handling Research Center, Stillwater, Oklahoma, June, 1999, pp. 443-459.
25. Swanson, R. P., "Lateral Dynamics of Non-Uniform Webs," Proceedings of the 10th International Conference on Web Handling, Web Handling Research Center, Stillwater, Oklahoma, June, 2009, pp. 531-554.